ACS APPLIED MATERIALS & INTERFACES

Research Article

www.acsami.org

Liquid Metal/Metal Oxide Frameworks with Incorporated Ga_2O_3 for Photocatalysis

Wei Zhang,*[,†] Boddu S. Naidu,[‡] Jian Zhen Ou,[†] Anthony P. O'Mullane,[§] Adam F. Chrimes,[†] Benjamin J. Carey,[†] Yichao Wang,[†] Shi-Yang Tang,[†] Vijay Sivan,[†] Arnan Mitchell,[†] Suresh K. Bhargava,[∥] and Kourosh Kalantar-zadeh*[,†]

[†]School of Electrical and Computer Engineering, RMIT University, Melbourne VIC 3001, Australia

[‡]Chemistry and Physics of Materials Unit, International Centre for Materials Science, Jawaharlal Nehru Centre for Advanced Scientific Research, Jakkur P. O., Bangalore 560 064, India

[§]School of Chemistry, Physics and Mechanical Engineering, Queensland University of Technology, Brisbane QLD 4001, Australia

[∥]School of Applied Sciences, RMIT University, Melbourne VIC 3001, Australia

Supporting Information

ABSTRACT: Solvothermally synthesized Ga_2O_3 nanoparticles are incorporated into liquid metal/metal oxide (LM/MO) frameworks in order to form enhanced photocatalytic systems. The LM/MO frameworks, both with and without incorporated Ga_2O_3 nanoparticles, show photocatalytic activity due to a plasmonic effect where performance is related to the loading of Ga_2O_3 nanoparticles. Optimum photocatalytic efficiency is obtained with 1 wt % incorporation of Ga_2O_3 nanoparticles. This can be attributed to the sub-bandgap states of LM/MO frameworks, contributing to pseudo-ohmic contacts which reduce the free carrier injection barrier to Ga_2O_3.

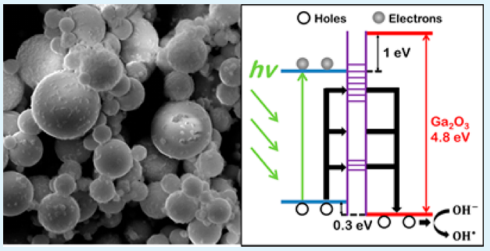

KEYWORDS: *liquid metal, galinstan, gallium oxide, photocatalysis*

1. INTRODUCTION

Liquid metals belong to the family of low-melting-point materials that maintain a liquid state at near room temperature. For years, mercury was the most used liquid metal; however, mercury's high toxicity has resulted in its gradual phasing out for many applications. Nowadays, gallium-based alloys, such as eutectic gallium–indium (EGaIn) and galinstan, are increasingly being used as replacements of mercury in different applications due to their relatively lower toxicity.[1,2] They provide relatively lower vapor pressures in comparison to mercury, and the formation of a thin layer of oxide (mainly made of gallium oxide) around the gallium-based alloys, in the presence of air, is another point of difference between these liquid metals and mercury that provides opportunities for creating advanced systems in microfluidics,[3−5] electronics,[6−8] self-healing devices,[9,10] and optics.[11,12]

With increasing global concerns regarding environmental remediation, the implementation of solar light driven metal/metal oxide photocatalysts for the decomposition of pollutants has drawn great interest.[13−15] The photocatalytic performance of such systems can be influenced by many factors including the efficiency of electron–hole pair generation and separation,[16−18] as well as the oxidizing potentials of the photogenerated charges.[19] The former is relevant to the bandgap and how facile the electron–hole pair can be separated. The latter is determined by the band position of the metal oxide component.[20] The ideal metal oxides in such a system are those with valence band edges exceeding the H_2O/O_2 oxidation potential, and with bandgap energies capable of absorbing the full solar light spectrum.

A wide bandgap metal oxide like gallium oxide (Ga_2O_3) has the advantage of providing photogenerated charges with high oxidizing potentials given that its valence band edge is found to be located at −7.75 eV vs vacuum.[21] However, photocatalytic applications of Ga_2O_3 are considerably limited on the grounds that it fails to generate sufficient electron–hole pairs upon illumination by solar light, as it has a wide band gap reported to be ∼4.8 eV.[21] Different approaches have been reported to form a metal/Ga_2O_3 system in order to enhance its photocatalytic activity. One of the most popular methods is to use noble metal nanoparticles to increase visible light absorption, by taking advantage of the surface plasmon resonance effect,[22] which has yet to be fully understood. Another approach is to dope metal ions into Ga_2O_3, but this inevitably prejudices the advantage of a highly negative conduction band edge.[23,24]

Recently, we reported the formation of liquid metal/metal oxide (LM/MO) frameworks.[25] These frameworks are films made of micro- to nanosized liquid metal galinstan spheres coated with nanosized metal oxides. Galinstan is a eutectic alloy of gallium, indium, and tin that naturally forms an oxide layer on its surface. Micro- to nanosized spheres in LM/MO frameworks can be made using a simple sonication technique.[25]

Received: November 5, 2014
Accepted: December 26, 2014
Published: December 26, 2014

DOI: 10.1021/am5077364
ACS Appl. Mater. Interfaces 2015, 7, 1943−1948

The loading of incorporated metal oxides can also be engineered on demand.[26,27] We have also demonstrated that LM/MO frameworks are capable of efficiently utilizing the solar spectrum as well as preserving metallic features that contribute to charge separation upon illumination. In light of this, with the majority of LM/MO frameworks consisting of gallium (68 wt % Ga, 22 wt % In, and 10 wt % Sn) in the purely metallic state, and knowing that Ga_2O_3 has a favorable valence band edge, it is hypothesized that an efficient LM/MO photocatalytic system can be potentially made of such frameworks upon the incorporation of additional Ga_2O_3.

In this work, we develop a combined system made of LM/MO frameworks and incorporated Ga_2O_3. We investigate the methods for improving its photocatalytic performance by incorporating different loadings of Ga_2O_3. Experimental details are in the Supporting Information.

2. RESULTS AND DISCUSSION

The suspension of micro- to nanosized liquid metal marble spheres is prepared by sonicating bulk galinstan in DI water (Figure 1a and b). A thick film of LM/MO frameworks is prepared by drop casting. Scanning electron microscopy (SEM) images of the cross section of the drop casted LM/MO frameworks film is shown in Figure S1 (Supporting Information). The Ga_2O_3 nanoparticles are synthesized using a solvothermal process.[28] Different amounts of Ga_2O_3 nanoparticles are incorporated onto these galinstan spheres, via co-sonication, in order to realize a variation of loading ratios. SEM images of LM/MO frameworks with and without an incorporated Ga_2O_3 nanoparticle coating can be seen in Figure 1c and d, respectively. The inset of Figure 1d shows that before incorporating Ga_2O_3 nanoparticles the LM/MO frameworks consist of micro- to nanosized galinstan spheres with native sub-stoichiometric oxides that originate through the sonication process.[25] Figure 1e shows the transmission electron microscopy (TEM) image of Ga_2O_3 nanoparticles which are synthesized using a solvothermal process where the dimension of most of the Ga_2O_3 nanoparticles is within the range of 5−10 nm. Figure 1f shows the corresponding selected area electron diffraction (SAED) pattern of Ga_2O_3 nanoparticles. The synthesized Ga_2O_3 is detected to be γ-Ga_2O_3 using X-ray diffraction (XRD) measurements (Figure S2, Supporting Information).

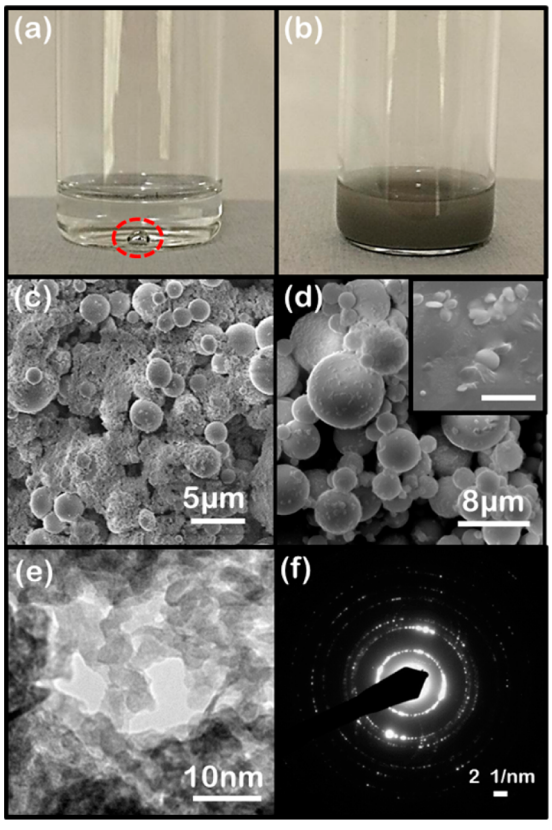

Figure 1. (a) A bulk galinstan droplet kept in DI water. (b) Suspension of micro- to nanosized liquid metal marble spheres. SEM images of (c) the top view of LM/MO frameworks with incorporated Ga_2O_3 nanoparticles (1 wt %) and (d) LM/MO frameworks without incorporated Ga_2O_3 nanoparticles (the inset shows native oxide nanoplatelets; the scale bar of the inset is 500 nm). (e) TEM image of solvothermally synthesized Ga_2O_3 nanoparticles. (f) TEM diffraction patterns of Ga_2O_3 nanoparticles.

Parts a−d of Figure 2 show the surface morphology of microsized galinstan spheres incorporated with different loadings of Ga_2O_3 nanoparticles. In Figure 2a, only the native surface oxide layer and native oxide nanoplatelets formed by the sonication process are observed, with zero loading of Ga_2O_3 nanoparticles. Figure 2b shows that Ga_2O_3 nanoparticles form a relatively uniform distribution on the spherical structure. Increasing the loading of Ga_2O_3 nanoparticles results in a reasonably uniform coating (Figure 2c). From Figure 2d, it is observed that most of the sphere surface is covered by Ga_2O_3 nanoparticles when the loading reaches 2 wt %. Low magnification SEM images are presented to show the surface morphology with respect to different loadings of Ga_2O_3 nanoparticles (Figure S3, Supporting Information).

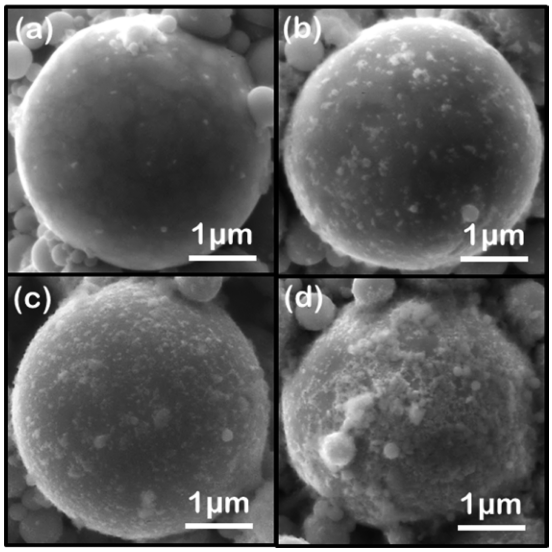

Figure 2. SEM images of the surface morphology of microsized galinstan spheres with different loadings of Ga_2O_3: (a) 0 wt %, (b) 0.2 wt %, (c) 1 wt %, and (d) 2 wt %.

To further characterize the effect of Ga_2O_3 nanoparticles incorporation, we conducted X-ray photoelectron spectroscopy (XPS) measurements of the LM/MO frameworks with various loadings of Ga_2O_3 nanoparticles. In the Ga 3d core level spectra (Figure 3a−e), peaks corresponding to Ga^{3+} (colored as red) and Ga^0 (colored as blue) are observed.[29] With the increase of Ga_2O_3 nanoparticles, the intensity of Ga^{3+} rises, while the

DOI: 10.1021/am5077364
ACS Appl. Mater. Interfaces 2015, 7, 1943−1948

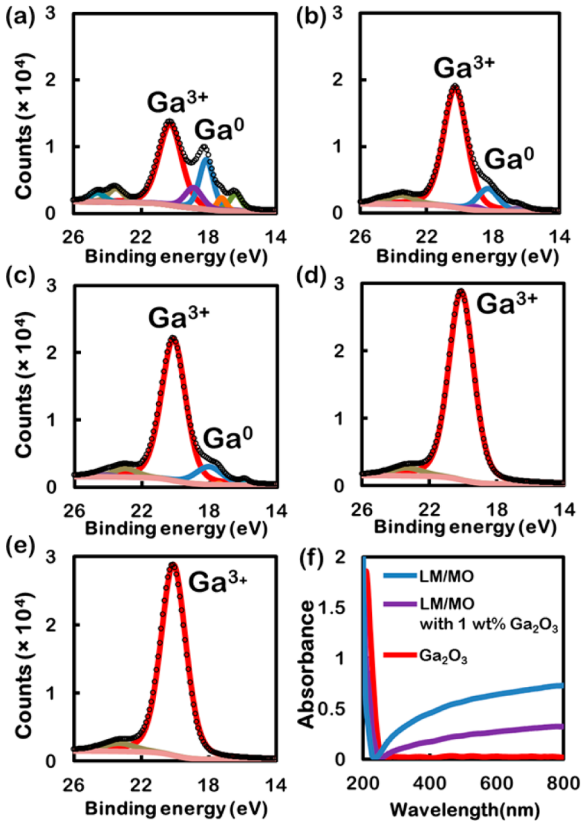

Figure 3. XPS spectra of Ga 3d of LM/MO frameworks with different loadings of Ga_2O_3 nanoparticles: (a) 0 wt %, (b) 0.2 wt %, (c) 1 wt %, and (d) 2 wt %. (e) The XPS spectrum of Ga 3d of solvothermally synthesized Ga_2O_3 nanoparticles. (f) UV−vis absorption spectra of Ga_2O_3 nanoparticles, LM/MO framework, and LM/MO framework with 1 wt % Ga_2O_3 nanoparticles.

intensity of Ga^0 decreases. The Ga^0 signal can originate from the core metal as well as the presence of metallic gallium in sub-stoichiometric gallium oxide nanoplatelets and the native oxide layer of LM/MO frameworks. As a result, XPS analysis suggests that it is likely that the incorporation of Ga_2O_3 nanoparticles changes the stoichiometry of the combined system at the contact boundaries between the metal and nanoparticles (this hypothesis is investigated further using XPS valence band measurements, and is presented later). UV−visible (UV−vis) spectroscopy is implemented to assess the absorbance of LM/MO frameworks with incorporation of Ga_2O_3 nanoparticles. LM/MO frameworks with the incorporation of 1 wt % Ga_2O_3 nanoparticles is chosen for analysis, as it presents a median phase between LM/MO frameworks and Ga_2O_3 nanoparticles used for the incorporation, according to the XPS spectra. Figure 3f shows that there is a strong signal in the deep UV region at less than 220 nm in the absorption spectrum of LM/MO frameworks. The strong signal can be ascribed to the surface plasmon resonances (SPR) of metallic submicron- or nanosized galinstan spheres.[30] The broad absorption peak spanning the UV and visible wavelengths could be attributed to plasmonic responses from the quasi-metallic sub-stoichiometric gallium oxides inherently formed on the surface of the spheres. The cutoff wavelength of the synthesized Ga_2O_3 nanoparticles is 260 nm; therefore, the corresponding bandgap of the Ga_2O_3 nanoparticles is estimated to be ∼4.8 eV. The UV spectrum of LM/MO frameworks incorporated with 1 wt % Ga_2O_3 nanoparticles lies in between the spectra of LM/MO frameworks and Ga_2O_3 nanoparticles, which is consistent with the result from XPS measurements. The spectrum of the combined system also has a broad absorption peak over UV and visible range. This shows that the system is also capable of efficiently absorbing light. The UV−vis reflectance and transmission spectra of LM/MO frameworks with 1 wt % Ga_2O_3 nanoparticles are shown in Figure S4 of the Supporting Information (a brief analysis of the data is presented in section S4 of the Supporting Information).

Congo red (CR) is utilized as the indicative dye to evaluate the photocatalytic performances of LM/MO frameworks incorporated with different concentrations of Ga_2O_3 nanoparticles. Additionally, samples made of pristine Ga_2O_3 and LM/MO frameworks are used as the benchmarks. As shown in Figure 4a, it is clearly seen that the pristine γ-Ga_2O_3 only decomposes CR at a rate of ∼0.03% h^{-1} under simulated solar light irradiation, which is attributed to its poor absorption in the solar spectrum owing to its wide energy band gap (∼4.8 eV). The decomposition efficiency of LM/MO frameworks toward CR is close to ∼47% h^{-1}, which is consistent with our previous work.[25] Significantly, the incorporation of Ga_2O_3 nanoparticles into the framework enhances the photocatalytic performance. Starting with as small a concentration as 0.2 wt % Ga_2O_3, the combined system reaches a CR decomposition rate

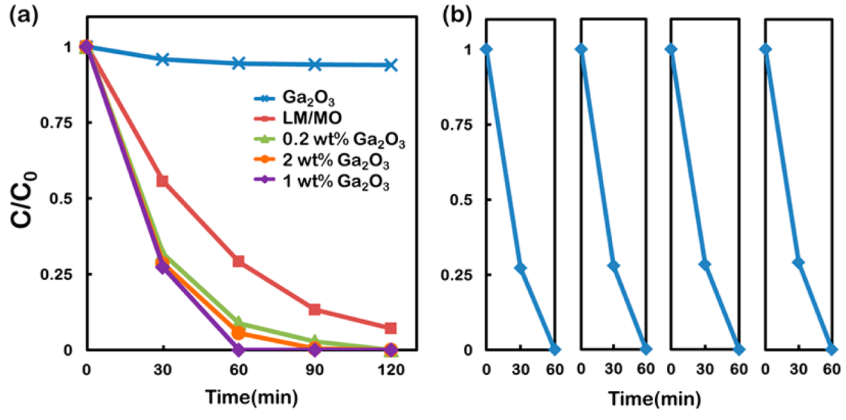

Figure 4. (a) Degradation of 10 μM CR in the presence of Ga_2O_3 nanoparticles, LM/MO frameworks, and LM/MO frameworks incorporated with different loadings of Ga_2O_3 nanoparticles. (b) Degradation of 10 μM CR in the presence of one sample of LM/MO frameworks with 1 wt % incorporated Ga_2O_3 in four consecutive cycles. The difference of decomposition rates among four consecutive cycles is less than 2%.

DOI: 10.1021/am5077364
ACS Appl. Mater. Interfaces 2015, 7, 1943−1948

of 50% h^{-1}. As the amount of Ga_2O_3 increases to 1 wt %, complete decomposition of CR is achieved within 1 h (~100% h^{-1}). Interestingly, further increasing the Ga_2O_3 coating to 2 wt % compromises the performance. It can be observed that the time duration for the complete decomposition of CR rises to 90 min (~67% h^{-1}). More photocatalytic activity responses can be found in Figure S5 (Supporting Information). Figure 4b shows the photocatalytic kinetic curves for the same LM/MO frameworks incorporated with 1 wt % Ga_2O_3 for four consecutive cycles. No significant degradation of CR decomposition efficiency during four consecutive cycles can be observed, confirming excellent stability and reusability of the system for photocatalytic applications. Raw data is presented in Table S1 (Supporting Information). Also, aluminum particles with incorporated Ga_2O_3 nanoparticles are chosen as a control experiment for photocatalytic activity. The outcomes are presented in Figure S6 (Supporting Information).

The enhancement in photocatalytic activity of the combined system can be related to its band position. The conduction and valence band positions of LM/MO frameworks and Ga_2O_3 nanoparticles are characterized using Mott–Schottky and XPS, respectively. From the Mott–Schottky plots shown in Figure 5a, the flat band potential of Ga_2O_3 nanoparticles is ~1.0 V more negative than that of LM/MO frameworks, which indicates that the conduction band edge of γ-Ga_2O_3 is ~1.0 eV more positive than that of the frameworks.[31,32] Linear sweeps and cyclic voltammograms are also obtained, and the results are shown in Figures S7 and S8 (Supporting Information). From Figure 5b, the difference in XPS valence band binding energy shows that the valence band edge of Ga_2O_3 is 0.3 eV more positive than that of the frameworks. As the band gap of Ga_2O_3 is ~4.8 eV, we therefore estimate that the overall band gap of LM/MO frameworks is ~3.5 eV. XPS valence band spectra of LM/MO frameworks with different Ga_2O_3 nanoparticle loadings are shown in Figure S9 (Supporting Information), which shows the gradual variation of difference between the Fermi level and valence band.

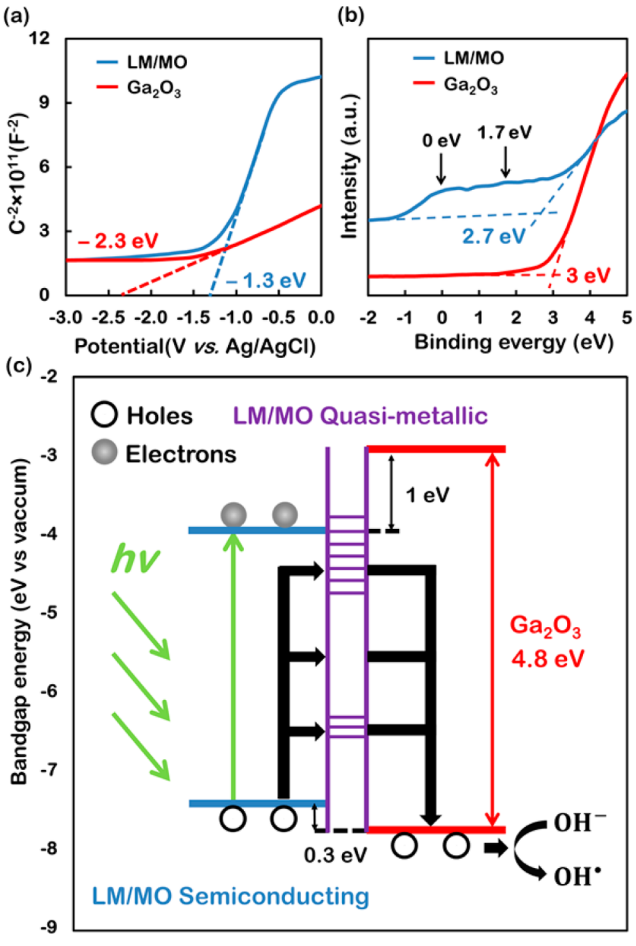

Figure 5. (a) Mott–Schottky plots of LM/MO frameworks and Ga_2O_3 nanoparticles measured in Na_2SO_4 solution (0.3 M, pH 7.0). (b) XPS valence band spectra of LM/MO frameworks and Ga_2O_3 nanoparticles. (c) Band structure diagram of the combined system.

From Figure 5b, it is noted that in the XPS valence spectrum of LM/MO frameworks there are two sub-bandgap states centered at 0 and 1.7 eV. Such sub-bandgap states could originate from oxygen vacancies in the sub-stoichiometric native oxides.[33] Therefore, this quasi-metallic part of the frameworks with dominant sub-bandgap states can potentially lead to the formation of pseudo-ohmic contacts in the vicinity of both the semiconducting part of the frameworks and the Ga_2O_3 nanoparticles, facilitating free carrier transfer.[34]

The enhancement of photocatalytic performance for the LM/MO framework incorporated with 1 wt % Ga_2O_3, in comparison to the performance of the LM/MO framework without Ga_2O_3 incorporation, is also due to another concurring effect as the plasmon peak decreases after incorporation of Ga_2O_3 (Figure 3f). To describe the photocatalytic performance, a band structure diagram of the combined system is shown in Figure 5c. We assume that, upon irradiation, a considerable amount of electron–hole pairs are generated in the semiconducting part of the frameworks. Because of the observation of broad peaks in the UV–vis measurements, a plasmonic effect should play a role in absorbing light in the UV–vis region in comparison to only Ga_2O_3 nanoparticles. In light of the pseudo-ohmic contacts induced by the quasi-metallic part of the LM/MO frameworks, the free carrier injection barrier is significantly reduced, therefore allowing nearly free transfer of holes from the frameworks to the valence band of Ga_2O_3 nanoparticles, where the holes have a higher oxidizing potential. Therefore, this promotes the decomposition of organic species. At the same time, electrons could either transfer to the liquid metal core or remain in the quasi-metallic part of the LM/MO frameworks, thus achieving efficient charge separation.

The variation of overall photocatalytic performance according to the concentration of incorporated Ga_2O_3 can be explained by a competition between two factors. On the one hand, incorporating Ga_2O_3 nanoparticles enhances the photocatalytic performance of the combined system due to enabling the higher oxidation potential of the holes which are transferred from the semiconducting part of the LM/MO frameworks through the pseudo-ohmic contacts which is facilitated by the presence of quasi-metallic features. On the other hand, the incorporation of Ga_2O_3 nanoparticles, which has a poor solar spectrum absorbability compared to LM/MO frameworks, inevitably reduces the available areas of the semiconducting part of the frameworks for efficient generation of electron–hole pairs, thus reducing the overall photocatalytic performance of the combined system. This is evidenced by the lower rate of CR photodecomposition of the combined system when the Ga_2O_3 loading exceeds 1 wt % (Figure 4a).

DOI: 10.1021/am5077364
ACS Appl. Mater. Interfaces 2015, 7, 1943–1948

3. CONCLUSION

In summary, γ-Ga_2O_3 nanoparticles were synthesized using a solvothermal process. Different loadings of Ga_2O_3 nanoparticles were incorporated into LM/MO frameworks made of micro- to nanosized galinstan spheres. The photocatalytic performance of the combined system was investigated by decomposing CR under illumination of simulated solar light. It was shown that potentially the plasmonic properties of the frameworks play an important role in their photocatalytic activities. However, it was observed that a concurrent phenomenon helped the LM/MO frameworks with 1 wt % incorporated Ga_2O_3 nanoparticles to demonstrate the optimum photocatalytic efficiency of ∼100% h^{-1} with high reusability, as shown by consecutive catalytic cycles. The investigation of the band structures of Ga_2O_3 nanoparticles and LM/MO frameworks revealed the potential formation of pseudo-ohmic contacts between the Ga_2O_3 nanoparticles and liquid metal components, reducing the hole injection barrier. As a result, the higher oxidizing potential and presence of an excess of holes at the valence band of Ga_2O_3 contributed to the enhancement of CR photodecomposition. The results show that LM/MO frameworks are capable of serving as a platform for Ga_2O_3 incorporation to significantly improve its photocataltyic performance and potentially being suitable for incorporating other wide bandgap semiconductors.

■ ASSOCIATED CONTENT

Ⓢ Supporting Information

Experimental details and supporting figures. This material is available free of charge via the Internet at http://pubs.acs.org.

■ AUTHOR INFORMATION

Corresponding Authors

*E-mail: s3342978@student.rmit.edu.com.
*E-mail: kourosh.kalantar@rmit.edu.au.

Notes

The authors declare no competing financial interest.

■ ACKNOWLEDGMENTS

The authors acknowledge the facilities, and the scientific and technical assistance, of the Australian Microscopy & Microanalysis Research Facility at the RMIT Microscopy & Microanalysis Facility, at RMIT University.

■ REFERENCES

(1) Dickey, M. D.; Chiechi, R. C.; Larsen, R. J.; Weiss, E. A.; Weitz, D. A.; Whitesides, G. M. Eutectic Gallium-Indium (EGaIn): A Liquid Metal Alloy for the Formation of Stable Structures in Microchannels at Room Temperature. *Adv. Funct. Mater.* **2008**, *18*, 1097−1104.

(2) Surmann, P.; Zeyat, H. Voltammetric Analysis using a Self-Renewable Non-Mercury Electrode. *Anal. Bioanal. Chem.* **2005**, *383*, 1009−1013.

(3) Krupenkin, T.; Taylor, J. A. Reverse Electrowetting as a New Approach to High-Power Energy Harvesting. *Nat. Commun.* **2011**, *2*, 448.

(4) Tang, S.-Y.; Sivan, V.; Khoshmanesh, K.; O'Mullane, A. P.; Tang, X.; Gol, B.; Eshtiaghi, N.; Lieder, F.; Petersen, P.; Mitchell, A. Electrochemically Induced Actuation of Liquid Metal Marbles. *Nanoscale* **2013**, *5*, 5949−5957.

(5) Tang, S.-Y.; Khoshmanesh, K.; Sivan, V.; Petersen, P.; O'Mullane, A. P.; Abbott, D.; Mitchell, A.; Kalantar-zadeh, K. Liquid Metal Enabled Pump. *Proc. Natl. Acad. Sci. U. S. A.* **2014**, *111*, 3304−3309.

(6) Ladd, C.; So, J. H.; Muth, J.; Dickey, M. D. 3D Printing of Free Standing Liquid Metal Microstructures. *Adv. Mater.* **2013**, *25*, 5081−5085.

(7) Park, J.; Wang, S.; Li, M.; Ahn, C.; Hyun, J. K.; Kim, D. S.; Kim, D. K.; Rogers, J. A.; Huang, Y.; Jeon, S. Three-Dimensional Nanonetworks for Giant Stretchability in Dielectrics and Conductors. *Nat. Commun.* **2012**, *3*, 916.

(8) Tang, S. Y.; Sivan, V.; Petersen, P.; Zhang, W.; Morrison, P. D.; Kalantar-zadeh, K.; Mitchell, A.; Khoshmanesh, K. Liquid Metal Actuator for Inducing Chaotic Advection. *Adv. Funct. Mater.* **2014**, *24*, 5851−5858.

(9) Palleau, E.; Reece, S.; Desai, S. C.; Smith, M. E.; Dickey, M. D. Self-Healing Stretchable Wires for Reconfigurable Circuit Wiring and 3D Microfluidics. *Adv. Mater.* **2013**, *25*, 1589−1592.

(10) Blaiszik, B. J.; Kramer, S. L.; Grady, M. E.; McIlroy, D. A.; Moore, J. S.; Sottos, N. R.; White, S. R. Autonomic Restoration of Electrical Conductivity. *Adv. Mater.* **2012**, *24*, 398−401.

(11) Mohammed, M. G.; Dickey, M. D. Strain-Controlled Diffraction of Light from Stretchable Liquid Metal Micro-Components. *Sens. Actuators, A* **2013**, *193*, 246−250.

(12) Wang, J.; Liu, S.; Vardeny, Z. V.; Nahata, A. Liquid Metal-Based Plasmonics. *Opt. Express* **2012**, *20*, 2346−2353.

(13) Li, H.; Bian, Z.; Zhu, J.; Huo, Y.; Li, H.; Lu, Y. Mesoporous Au/TiO_2 Nanocomposites with Enhanced Photocatalytic Activity. *J. Am. Chem. Soc.* **2007**, *129*, 4538−4539.

(14) Su, R.; Tiruvalam, R.; He, Q.; Dimitratos, N.; Kesavan, L.; Hammond, C.; Lopez-Sanchez, J. A.; Bechstein, R.; Kiely, C. J.; Hutchings, G. J.; Besenbacher, F. Promotion of Phenol Photo-decomposition over TiO_2 Using Au, Pd, and Au−Pd Nanoparticles. *ACS Nano* **2012**, *6*, 6284−6292.

(15) Formo, E.; Lee, E.; Campbell, D.; Xia, Y. Functionalization of Electrospun TiO_2 Nanofibers with Pt Nanoparticles and Nanowires for Catalytic Applications. *Nano Lett.* **2008**, *8*, 668−672.

(16) Hirakawa, T.; Kamat, P. V. Charge Separation and Catalytic Activity of Ag@ TiO_2 Core-Shell Composite Clusters under UV-Irradiation. *J. Am. Chem. Soc.* **2005**, *127*, 3928−3934.

(17) Yu, C.; Yang, K.; Xie, Y.; Fan, Q.; Jimmy, C. Y.; Shu, Q.; Wang, C. Novel Hollow Pt-ZnO Nanocomposite Microspheres with Hierarchical Structure and Enhanced Photocatalytic Activity and Stability. *Nanoscale* **2013**, *5*, 2142−2151.

(18) Shanmugam, S.; Gabashvili, A.; Jacob, D. S.; Yu, J. C.; Gedanken, A. Synthesis and Characterization of TiO_2@C Core-Shell Composite Nanoparticles and Evaluation of Their Photocatalytic Activities. *Chem. Mater.* **2006**, *18*, 2275−2282.

(19) Li, Y.; Wang, W.-N.; Zhan, Z.; Woo, M.-H.; Wu, C.-Y.; Biswas, P. Photocatalytic Reduction of CO_2 with H_2O on Mesoporous Silica Supported Cu/TiO_2 Catalysts. *Appl. Catal., B* **2010**, *100*, 386−392.

(20) HoonáChoi, J.; MináChoi, K.; KiáLee, D.; KuáKang, J. Highly Porous Gallium Oxide with a High CO_2 Affinity for the Photocatalytic Conversion of Carbon Dioxide into Methane. *J. Mater. Chem.* **2012**, *22*, 5304−5307.

(21) Qiao, L.; Su, F.; Bi, H.; Girault, H. H.; Liu, B. Ga_2O_3 Photocatalyzed On-Line Tagging of Cysteine to Facilitate Peptide Mass Fingerprinting. *Proteomics* **2011**, *11*, 3501−3509.

(22) Chen, P.-H.; Hsieh, C.-H.; Chen, S.-Y.; Wu, C.-H.; Wu, Y.-J.; Chou, L.-J.; Chen, L.-J. Direct Observation of Au/Ga_2O_3 Peapodded Nanowires and Their Plasmonic Behaviors. *Nano Lett.* **2010**, *10*, 3267−3271.

(23) Sakata, Y.; Matsuda, Y.; Yanagida, T.; Hirata, K.; Imamura, H.; Teramura, K. Effect of Metal Ion Addition in a Ni Supported Ga_2O_3 Photocatalyst on the Photocatalytic Overall Splitting of H_2O. *Catal. Lett.* **2008**, *125*, 22−26.

(24) Wang, X.; Shen, S.; Jin, S.; Yang, J.; Li, M.; Wang, X.; Han, H.; Li, C. Effects of Zn^{2+} and Pb^{2+} Dopants on the Activity of Ga_2O_3-Based Photocatalysts for Water Splitting. *Phys. Chem. Chem. Phys.* **2013**, *15*, 19380−19386.

(25) Zhang, W.; Ou, J. Z.; Tang, S. Y.; Sivan, V.; Yao, D. D.; Latham, K.; Khoshmanesh, K.; Mitchell, A.; O'Mullane, A. P.; Kalantar-zadeh, K. Liquid Metal/Metal Oxide Frameworks. *Adv. Funct. Mater.* **2014**, *24*, 3799−3807.

DOI: 10.1021/am5077364
ACS Appl. Mater. Interfaces 2015, 7, 1943−1948

(26) Sivan, V.; Tang, S.-Y.; O'Mullane, A. P.; Petersen, P.; Eshtiaghi, N.; Kalantar-zadeh, K.; Mitchell, A. Liquid Metal Marbles. *Adv. Funct. Mater.* **2013**, *23*, 144−152.
(27) Tang, X.; Tang, S.-Y.; Sivan, V.; Zhang, W.; Mitchell, A.; Kalantar-zadeh, K.; Khoshmanesh, K. Photochemically Induced Motion of Liquid Metal Marbles. *Appl. Phys. Lett.* **2013**, *103*, 174104.
(28) Sinha, G.; Patra, A. Generation of Green, Red and White Light from Rare-Earth Doped Ga_2O_3 Nanoparticles. *Chem. Phys. Lett.* **2009**, *473*, 151−154.
(29) Surdu-Bob, C. C.; Saied, S. O.; Sullivan, J. L. An X-ray Photoelectron Spectroscopy Study of the Oxides of GaAs. *Appl. Surf. Sci.* **2001**, *183*, 126−136.
(30) Hohman, J. N.; Kim, M.; Wadsworth, G. A.; Bednar, H. R.; Jiang, J.; LeThai, M. A.; Weiss, P. S. Directing Substrate Morphology via Self-Assembly: Ligand-Mediated Scission of Gallium−Indium Microspheres to the Nanoscale. *Nano Lett.* **2011**, *11*, 5104−5110.
(31) Wang, X.; Xu, Q.; Li, M.; Shen, S.; Wang, X.; Wang, Y.; Feng, Z.; Shi, J.; Han, H.; Li, C.; Photocatalytic Overall, Water Splitting Promoted by an $\alpha-\beta$ phase Junction on Ga_2O_3. *Angew. Chem., Int. Ed.* **2012**, *51*, 13089−13092.
(32) Ju, M.-G.; Wang, X.; Liang, W.; Zhao, Y.; Li, C. Tuning Energy Band-Gap of Gallium Oxide Crystalline to Enhance Photoelectrochemical Water Splitting: Mixed-Phase Junctions. *J. Mater. Chem. A* **2014**, *2*, 17005−17014.
(33) Porte, L. Electronic Structure of Non-Stoichiometric Zirconium Nitrides ZrNx. *Solid State Commun.* **1984**, *50*, 303−306.
(34) Vasilopoulou, M.; Papadimitropoulos, G.; Palilis, L. C.; Georgiadou, D. G.; Argitis, P.; Kennou, S.; Kostis, I.; Vourdas, N.; Stathopoulos, N. A.; Davazoglou, D. High Performance Organic Light Emitting Diodes using Substoichiometric Tungsten Oxide as Efficient Hole Injection Layer. *Org. Electron.* **2012**, *13*, 796−806.

DOI: 10.1021/am5077364
ACS Appl. Mater. Interfaces 2015, 7, 1943−1948